Geometry-specified troposphere decorrelation for subcentimeter real-time kinematic solutions over long baselines

Bofeng Li,[1,2,3] Yanming Feng,[2] Yunzhong Shen,[1,3] and Charles Wang[2]

Received 16 March 2010; revised 3 July 2010; accepted 3 August 2010; published 10 November 2010.

[1] Real-time kinematic (RTK) GPS techniques have been extensively developed for applications including surveying, structural monitoring, and machine automation. Limitations of the existing RTK techniques that hinder their applications for geodynamics purposes are twofold: (1) the achievable RTK accuracy is on the level of a few centimeters and the uncertainty of vertical component is 1.5–2 times worse than those of horizontal components and (2) the RTK position uncertainty grows in proportional to the base-to-rover distances. The key limiting factor behind the problems is the significant effect of residual tropospheric errors on the positioning solutions, especially on the highly correlated height component. This paper develops the geometry-specified troposphere decorrelation strategy to achieve the subcentimeter kinematic positioning accuracy in all three components. The key is to set up a relative zenith tropospheric delay (RZTD) parameter to absorb the residual tropospheric effects and to solve the established model as an ill-posed problem using the regularization method. In order to compute a reasonable regularization parameter to obtain an optimal regularized solution, the covariance matrix of positional parameters estimated without the RZTD parameter, which is characterized by observation geometry, is used to replace the quadratic matrix of their "true" values. As a result, the regularization parameter is adaptively computed with variation of observation geometry. The experiment results show that new method can efficiently alleviate the model's ill condition and stabilize the solution from a single data epoch. Compared to the results from the conventional least squares method, the new method can improve the long-range RTK solution precision from several centimeters to the subcentimeter in all components. More significantly, the precision of the height component is even higher. Several geosciences applications that require subcentimeter real-time solutions can largely benefit from the proposed approach, such as monitoring of earthquakes and large dams in real-time, high-precision GPS leveling and refinement of the vertical datum. In addition, the high-resolution RZTD solutions can contribute to effective recovery of tropospheric slant path delays in order to establish a 4-D troposphere tomography.

Citation: Li, B., Y. Feng, Y. Shen, and C. Wang (2010), Geometry-specified troposphere decorrelation for subcentimeter real-time kinematic solutions over long baselines, *J. Geophys. Res.*, *115*, B11404, doi:10.1029/2010JB007549.

1. Introduction

[2] Global Navigation Satellite Systems (GNSS) real-time kinematic (RTK) precise positioning technique has being extensively developed over the past two decades and widely used in the areas, such as geodesy, engineering and machine automation. The RTK solutions are determined without the need of user dynamic knowledge, thus being preferable in some geosciences applications [*Genrich and Bock*, 1992; *Bock et al.*, 2004; *Hofmann-Wellenhof and Moritz*, 2006; *Shi et al.*, 2010]. For instance, the high-rate GPS data can capture the rapid coseismic ground displacements over a range of frequencies and amplitudes that are in some sense wider than the seismic sensors can do. *Bock et al.* [2004] demonstrated its capability of detecting arbitrarily large dynamic ground motions and sensing seismic surface waves from several hundreds or even thousands of kilometers away. *Shi et al.* [2010] has successfully estimated the seismic displacement of the *Mw*8.0 Wenchuan earthquake from high-rate GPS observations. Other examples include the use of GPS RTK solutions for leveling and determination of local geoid surface model [*Hofmann-Wellenhof and Moritz*, 2006]. The limitations of the existing RTK techniques that hinder their applications in geosciences are twofold: (1) the achievable RTK accuracy remains in the level of a few centimeters and the uncertainty of the vertical component is

[1]Department of Surveying and Geo-informatics Engineering, Tongji University, Shanghai, China.
[2]Faculty of Science and Technology, Queensland University of Technology, Brisbane, Queensland, Australia.
[3]Key Laboratory of Advanced Surveying Engineering of State Bureau of Surveying and Mapping, Shanghai, China.

0148-0227/10/2010JB007549

1.5–2 times worse than those of the horizontal components; (2) the RTK position uncertainty grows in proportional to the base-to-rover distances [*Grejner-Brzezinska et al.*, 2005].

[3] The ionosphere and troposphere are considered as two key dominating error sources limiting the capability of carrier phase ambiguity resolution (AR) and the positional precision and accuracy [*Zhang and Lachapelle*, 2001; *Hu et al.*, 2003; *Kim et al.*, 2004; *Leick*, 2004; *Wielgosz et al.*, 2005; *Schüler*, 2006; *Ahn et al.*, 2008]. If the ambiguities are successfully fixed, the ionospheric influence on the position solutions can be basically eliminated using the ionosphere-free combination of dual-frequency GNSS signals. However, the tropospheric delay can never be reduced using additional frequencies [*Zhang and Lachapelle*, 2001; *Leick*, 2004; *Li et al.*, 2010]. The effects of tropospheric errors on position solutions depends on the base-to-rover distances, usually a few centimeters for the distances of a few tens of kilometers. With the future generation GNSS systems, the multiple frequency GNSS signals will be available for civilian use. The phase integer ambiguities on all carriers can be resolved reliably over the distances of hundreds of kilometers [*Li et al.*, 2010], and the tropospheric effects on position states can grow up to a few decimeters [*Li et al.*, 2010; *Feng and Li*, 2010]. Provided that the precise GNSS orbits are used instead of broadcast orbits, the troposphere would be the remaining dominating factor.

[4] A number of processing strategies have been used in dealing with tropospheric effects. The simplest strategy is to ignore the residual tropospheric errors over the short baselines where the tropospheric errors in two receivers are hypothetically correlated so that their effects can be basically canceled after the usual double differencing operation. For instance, in the traditional single-base RTK, the distance between a base station and a rover is typically restricted to 20 km or less in order to adequately cancel the residual atmospheric effects [*Dai et al.*, 2003; *Hu et al.*, 2003]. The network RTK is an alternative approach to mitigate the tropospheric errors, thus extending the service coverage. The relative tropospheric delays between multiple reference stations are used to interpolate the tropospheric errors between the master reference station and user within the network coverage [*Hu et al.*, 2003; *Chen et al.*, 2001; *Zhang and Lachapelle*, 2001; *Kim and Langley*, 2008]. Although the network RTK methods have been widely used in commercial services, the problem is when the interstation distances increase, the correlation of tropospheric errors at two stations decrease, the effects of the remaining tropospheric errors on the position estimation increases again. Therefore, the current dual-frequency based network-RTK systems restrict their interstation distances to 50–70 km albeit the distance limitation may be doubled using triple frequency receivers as shown by *Feng and Li* [2008]. In addition, the interpolated corrections for the rover become vulnerable to the localized anomalous errors under unfavorable atmospheric conditions [*Wielgosz et al.*, 2005; *Kim and Langley*, 2008; *Ahn et al.*, 2008]. The third approach is to set up a tropospheric parameter, such as relative zenith tropospheric delay (RZTD), to absorb the residual tropospheric effects and a filtering technique is usually employed [*Tralli and Lichten*, 1990; *Dodson et al.*, 1996; *Zhang and Lachapelle*, 2001]. This method can overcome the distance limitations. Instead, it works well over longer baselines, either in single-base or network-RTK situations.

[5] However, once the RZTD parameter is introduced along with coordinates, the model is seriously ill-conditioned due to its strong correlation with the height parameter as recognized by *Dodson et al.* [1996]. Thus, it cannot be precisely solved without enough observation accumulation. In general, the residual tropospheric delays are assumed of first-order Gauss-Markov random walk process, and a filtering technique, such as Kalman filtering, is often used. In a static scenario, the results from *Tralli and Lichten* [1990] suggest that a few minutes of GPS observations have the sufficient strength to resolve centimeter-level zenith delay fluctuations. In long-range RTK, *Kim and Langley* [2008] also use Kalman filtering to estimate the coordinates along with the filtered RZTD, where a forgetting factor is applied to weight the RZTD estimate at current epoch and the previously filtered estimates. However, the forgetting factor is governed by both temporal and spatial correlations, and then it is, to a great extent, empirically given. Furthermore, the filtered RZTD solutions cannot effectively reflect the real-time variation of troposphere environment. This is especially the case when user receivers experience complex atmospheric conditions or highly mobile environment. Therefore, an ideal approach is to precisely estimate all parameters independently in such ill-posed model epoch by epoch. The problem is how to mitigate the ill condition and to stabilize the epochwise solution. *Ahn et al.* [2008] combined RZTD and height together to estimate, and then their correlation coefficient was searched to separate RZTD and height. However, this method essentially specifies the correlation only between the RZTD and the height, and the correlations between the RZTD and the horizontal components are not adequately taken into account although they are relatively smaller.

[6] In an ill-posed problem, a small error in the observation will cause large error in the least squares (LS) estimate. In this study, we use regularization method to solve for the stable solution epoch by epoch without any dependency between epochs. Thus the solution can characterize the real-time variation of RZTD, and subcentimeter positional precision is obtained. The key is to compute a reasonable regularization parameter and then get an optimal regularized solution where the "true" values of parameters are involved but in fact impossibly known. In this study, we use the covariance matrix of position parameters from LS estimation without RZTD, which is specified by observation geometry, as a substitute of the quadratic matrix of "true" values. As a result, the regularization parameter is adaptively computed with variation of observation geometry, and the correlation between RZTD and height is effectively reduced.

[7] The rest of the paper is organized as follows. Section 2 begins with a brief review on the AR in RTK techniques. Then the mathematical model of ionosphere-free observation with RZTD and its LS solutions with and without RZTD are presented. In section 3, the regularization is introduced to compute stable solution in the ill-posed problem. The theory of regularization parameter determination is claimed using the covariance matrix of position parameters from LS esti-

mation without RZTD to replace the quadratic matrix of "true" values. Experimental results are presented in section 4 to demonstrate the performance of proposed method. Finally, we conclude the research findings and present the remarks.

2. Mathematical Model of Ionosphere-Free Combination With RZTD and LS Solutions

[8] We first give a brief review on the AR in current RTK techniques, and then proceed with the mathematical model of ionosphere-free combination based on the equivalent theory along with a RZTD. In addition, the LS solutions both with and without RZTD are given.

2.1. Real-Time Ambiguity Resolution in RTK Techniques

[9] So far, there are three representative RTK techniques, traditional (or standard) single-base RTK, network RTK and long-range (single-base) RTK, which correspond to three typical real-time AR strategies:

[10] 1. In traditional single-base RTK, the base-to-rover distance is generally restricted to no longer than 20 km such that the systematic errors remaining in the double differenced (DD) phase measurements are ignorable with respect to their wavelengths. Therefore the so-called on-the-fly techniques can be used to reliably fix the ambiguities in real time or near real time [see, e.g., *Frei and Beutler*, 1990; *Hatch*, 1990; *Teunissen*, 1995; *Li and Shen*, 2010].

[11] 2. The network RTK approach has been widely adopted for commercial services in the past decade, which can increase the reliability of a RTK system and extend its service area a few times. In this approach, the real-time AR over interstation baselines is the prerequisite to generate the network corrections for the users. Since the coordinates of reference stations are precisely known, the network AR is essentially the static AR in medium-distance baselines. The ionosphere-free model is always used and only ambiguities and a RZTD are unknown. The Kalman filtering procedure is used to reliably fix the ambiguities if their float solutions are sufficient close to integers after a few minutes filtering processing [*Chen et al.*, 2000; *Hu et al.*, 2003; *Dai et al.*, 2003].

[12] 3. The long-range (single-base) RTK technique has attracted considerable research attentions. Since the position parameters are varying epoch by epoch and the atmospheric errors vary in more dramatic and complex behavior, the underlying AR model is often weak. Thus it usually needs to accumulate many observation epochs to estimate the precise float ambiguities and then fix them to integers. To enhance the strength of AR model and also make the filtered RZTD consistent with the real-world situation, a forgetting factor is applied to down weight the RZTD estimates at the previous epoch as suggested by *Kim and Langley* [2008]. Although the filtered RZTD is actually the smoothed RZTD over multiple data epochs, it is sufficiently precise to recover the integer ambiguities if its uncertainty is far smaller than 0.5 cycles.

[13] In near future, the multiple frequency GNSS signals will be accessible and the ambiguities can be reliably solved in several minutes without distance constraint [*Li et al.*, 2010], which means that the AR is not a key barrier for long-range RTK anymore.

[14] Admittedly, AR is important for RTK positioning, but it is just an intermediate step to obtain the precise observations and then the precise position solutions. While most users seem to passively accept centimeter-level positioning accuracy as RTK system directly gives, little research attention has been paid to further improve the RTK precision after the ambiguity-fixed observations are obtained. In fact, this issue is not easier than AR itself for two reasons:

[15] 1. As far as integer estimation of AR is concerned, the ambiguities can be reliably fixed to their integers as long as the residual systematic errors are adequately mitigated. In other words, AR can tolerate a certain level of the systematic errors in the DD measurements. However, the remaining DD systematic errors will still affect the position solutions. The smaller the residual systematic errors, the more precise the RTK solutions.

[16] 2. For AR purpose, due to the constant nature of the ambiguities, measurements from multiple epochs can often be used to reliably determine the integers. The successful AR depends actually on the smoothed (or averaged) float ambiguities rather than float ambiguities from each epoch. The RTK position is however usually estimated with measurements of a single epoch without any assumption of user dynamics. This is the beauty of real-time kinematic positioning.

[17] It is generally noted that the centimeter RTK precision is achievable if the ambiguities are correctly fixed. This paper is motivated to further improve the long-range RTK precision after the DD phase ambiguities are correctly fixed. Therefore we focus our research concentration on the improved position estimation with the ambiguity-fixed observations.

2.2. DD Observation Equations With RZTD

[18] We start with the dual-frequency ambiguity-fixed DD GPS observation equations

$$\begin{cases} \Phi_1 = \rho + T - I_1 + \varepsilon_{\Phi_1} \\ \Phi_2 = \rho + T - f_1^2/f_2^2 \times I_1 + \varepsilon_{\Phi_2} \\ P_1 = \rho + T + I_1 + \varepsilon_{P_1} \\ P_2 = \rho + T + f_1^2/f_2^2 \times I_1 + \varepsilon_{P_2} \end{cases} \quad (1)$$

where the subscripts "1" and "2" represent the terms associated with L1 and L2 carriers; Φ and P are DD phase and code observations, respectively; ρ is the actual DD satellite-to-receiver distance; I_1 is the DD ionospheric delay at L1 frequency; T is the residual DD tropospheric delay corrected with UNB3 tropospheric standard model [*Collins and Langley*, 1997; *Kim et al.*, 2004] along with Niell mapping function [*Niell*, 1996; also see e.g., *Leick*, 2004]; ε is the random noise of normal distribution with zero mean; and f_1 and f_2 are frequency values at L1 and L2 carriers.

[19] The tropospheric delay is composed of hydrostatic and wet components, of which the hydrostatic delay contributes to more than 90% of the total delay and can be accurately modeled using the standard model. However, the wet delay is difficult to remove due to its more complex spatiotemporal variation [*Zhang and Lachapelle*, 2001; *Tralli and Lichten*, 1990; *Leick*, 2004]. Thus, the residual delay is mostly due to the wet component. We express the residual delay as a function of RZTD and wet mapping with assumption

of azimuthal symmetry [*Zhang and Lachapelle*, 2001; *Hu et al.*, 2003; *Dai et al.*, 2003],

$$T = (m^q - m^p) \times \tau = b \times \tau \tag{2}$$

where T is the residual tropospheric delay; τ is the RZTD parameter; m^q and m^p are Niell's wet mapping function [*Niell*, 1996] for satellite p and q. For example, m^p is expressed as

$$m^p = \frac{1 + \dfrac{d}{1 + e/e(1+g)}}{\sin\theta^p + \dfrac{d}{\sin\theta^p + e/(\sin\theta^p + g)}} \tag{3}$$

where θ^p is the average elevation angles of the two stations for satellites p and d, e, g are the coefficients and interpolated from tabular data [see, e.g., *Leick*, 2004].

[20] If there are $(m + 1)$ satellites being simultaneously tracked at an epoch, we have a collection of $4m$ observation equations in total:

$$\begin{bmatrix} \mathbf{\Phi}_1 \\ \mathbf{\Phi}_2 \\ \mathbf{P}_1 \\ \mathbf{P}_2 \end{bmatrix} = \begin{bmatrix} \mathbf{A} & \mathbf{b} & -\mathbf{E}_m \\ \mathbf{A} & \mathbf{b} & -f_1^2/f_2^2\mathbf{E}_m \\ \mathbf{A} & \mathbf{b} & \mathbf{E}_m \\ \mathbf{A} & \mathbf{b} & f_1^2/f_2^2\mathbf{E}_m \end{bmatrix} \begin{bmatrix} \mathbf{x} \\ \tau \\ \mathbf{I}_1 \end{bmatrix} + \begin{bmatrix} \varepsilon_{\Phi_1} \\ \varepsilon_{\Phi_2} \\ \varepsilon_{P_1} \\ \varepsilon_{P_2} \end{bmatrix} \tag{4}$$

where $\mathbf{\Phi}_1 = [\Phi_1^1 \cdots \Phi_1^m]^T$ and $\varepsilon_{\Phi 1} = [\varepsilon_{\Phi_1{}^1} \cdots \varepsilon_{\Phi_1{}^m}]^T$ are $(m \times 1)$ L1 DD phase observation and their noise vectors, respectively; $\mathbf{\Phi}_2$, $\mathbf{P}_1$ and $\mathbf{P}_2$ as well as $\varepsilon_{\Phi 2}$, ε_{P1} and ε_{P2} have the similar structures as $\mathbf{\Phi}_1$ and $\varepsilon_{\Phi 1}$, respectively; $\mathbf{A}$ is $(m \times 3)$ coefficient matrix for coordinate corrections $\mathbf{x} = [x\ y\ z]^T$ in WGS-84 coordinate system; $\mathbf{b}$ is the column coefficient vector of the RZTD parameter for all DD measurements; $\mathbf{I}_1 = [I_1^1 \cdots I_1^m]^T$ is column vector composed of m DD ionospheric delays with respect to L1 frequency; $\beta = f_1^2/(f_1^2 - f_2^2)$ and $\mathbf{E}_m$ is $(m \times m)$ identity matrix. For simplification of expression, we note that

$$\mathbf{y}_{DD} = \begin{bmatrix} \mathbf{\Phi}_1^T & \mathbf{\Phi}_2^T & \mathbf{P}_1^T & \mathbf{P}_2^T \end{bmatrix}^T \tag{5a}$$

$$\varepsilon_{DD} = \begin{bmatrix} \varepsilon_{\Phi_1}^T & \varepsilon_{\Phi_2}^T & \varepsilon_{P_1}^T & \varepsilon_{P_2}^T \end{bmatrix}^T \tag{5b}$$

Considering the following stochastic model of DD observations for one epoch [*Leick*, 2004]

$$\mathbf{\Sigma}_{\mathbf{y}_{DD}} = \sigma_{\Phi_1}^2 (\mathbf{\Lambda} \otimes \mathbf{Q}_{DD}) \tag{6a}$$

with scalar diagonal matrix

$$\mathbf{\Lambda} = \begin{bmatrix} 1 & & & \\ & s_{\Phi_2} & & \\ & & s_{P_1} & \\ & & & s_{P_2} \end{bmatrix} \tag{6b}$$

where

$$s_{\Phi_2} = \frac{\sigma_{\Phi_2}^2}{\sigma_{\Phi_1}^2},\ s_{P_1} = \frac{\sigma_{P_1}^2}{\sigma_{\Phi_1}^2},\ \text{and}\ s_{P_2} = \frac{\sigma_{P_2}^2}{\sigma_{\Phi_1}^2}$$

are variance ratios for L2, P1, and P2 observations relative to L1; $\sigma_{\Phi_1}^2$, $\sigma_{\Phi_2}^2$, $\sigma_{P_1}^2$, and $\sigma_{P_2}^2$ are variance components of undifferenced observations for different observation types, respectively. In the following, we use $\sigma_0^2 = \sigma_{\Phi_1}^2$ as variance component of unit weight. $\mathbf{Q}_{DD}$ is constant cofactor matrix for one type of DD observations of single epoch. If all observations are assumed to be independent and have a same variance, then

$$\mathbf{Q}_{DD} = 2 \times \left(\mathbf{e}_m \mathbf{e}_m^T + \mathbf{E}_m\right) \tag{7}$$

where $\mathbf{e}_m$ is an m column vector with all elements being one. In this study, an elevation-dependent weighting function is specified for determining variance of original observations [*Gendt et al.*, 2003]

$$p = \begin{cases} 1 & \theta > 30^\circ \\ 0.5/\sin(\theta) & \theta \le 30^\circ \end{cases} \tag{8}$$

In this case, the DD cofactor matrix can be rigorously derived according to the law of error propagation. In addition, a cross correlation between different observation types should be specified if it is significant and the reasonable weight matrix is desirable [*Li et al.*, 2008]. For instance, if the cross correlation between L1 and L2 phases is involved (denoted as $\rho_{\Phi_{1,2}}$), the scalar matrix (6b) becomes

$$\mathbf{\Lambda} = \begin{bmatrix} 1 & \rho_{\Phi_{1,2}}\sqrt{s_{\Phi_2}} & & \\ \rho_{\Phi_{1,2}}\sqrt{s_{\Phi_2}} & s_{\Phi_2} & & \\ & & s_{P_1} & \\ & & & s_{P_2} \end{bmatrix} \tag{9}$$

2.3. Ionosphere-Free Model Based on Equivalence Theory

[21] The ionospheric delay, traditionally one of the key limiting factors for precise positioning, can be basically eliminated by forming the ionosphere-free combination. According to the equivalent theory [*Schaffrin and Grafarend*, 1986; *Xu*, 2002; *Shen and Xu*, 2008; *Shen et al.*, 2009], the nuisance ionospheric delays are eliminated via multiplying an appropriate transformation matrix left to both sides of equation (4) without any influence on the remaining parameter estimation. The ionosphere-free transformation matrix ($\mathbf{T}$) is symbolized as

$$\mathbf{G} = \mathbf{T} \otimes \mathbf{E}_m \tag{10a}$$

where

$$\mathbf{T} = \begin{bmatrix} \beta & \gamma & 0 & 0 \\ 0 & \gamma/(\gamma - \beta) & \beta/(\beta - \gamma) & 0 \\ 0 & 0 & \beta & \gamma \end{bmatrix} \tag{10b}$$

with $\beta = f_1^2/(f_1^2 - f_2^2)$ and $\gamma = -f_2^2/(f_1^2 - f_2^2)$. After left multiplying equation (4) by $\mathbf{G}$, it yields the ionosphere-free error equations as

$$\mathbf{y}_{IF} = \begin{bmatrix} \mathbf{e}_3 \otimes \mathbf{A} & \mathbf{e}_3 \otimes \mathbf{b} \end{bmatrix} \begin{bmatrix} \mathbf{x} \\ \tau \end{bmatrix} + \varepsilon_{IF} \tag{11}$$

with $\mathbf{y}_{IF} = \mathbf{G}\mathbf{y}_{DD}$ and $\varepsilon_{IF} = \mathbf{G}\varepsilon_{DD}$. Accordingly, the covariance matrix for ionosphere-free observations is derived

$$\mathbf{\Sigma}_{\mathbf{y}_{IF}} = \mathbf{G}\mathbf{\Sigma}_{\mathbf{y}_{DD}}\mathbf{G}^T = \sigma_0^2\left(\mathbf{T}\mathbf{\Lambda}\mathbf{T}^T \otimes \mathbf{Q}_{DD}\right) = \sigma_0^2\mathbf{Q}_{IF} \tag{12}$$

If coordinate corrections are expressed in the topocentric coordinate system, i.e., $\mathbf{x} = [n\ e\ h]^T$, it is trivial to right

multiply the coefficient matrix **A** by a transformation matrix [*Leick*, 2004]

$$\mathbf{R} = \begin{pmatrix} -\sin\varphi\cos\lambda & -\sin\lambda & \cos\varphi\cos\lambda \\ -\sin\varphi\sin\lambda & \cos\lambda & \cos\varphi\sin\lambda \\ \cos\varphi & 0 & \sin\varphi \end{pmatrix} \tag{13}$$

where φ and λ are the nominal latitude and longitude of the topocentric station.

2.4. LS Solutions With and Without RZTD

[22] The error equations (11) are compactly rewritten as

$$\mathbf{y}_{IF} = \mathbf{H}\boldsymbol{\xi} + \varepsilon_{IF} \tag{14}$$

where $\mathbf{H} = [\mathbf{e}_3 \otimes \mathbf{A}\ \mathbf{e}_3 \otimes \mathbf{b}]$ and $\boldsymbol{\xi} = \begin{bmatrix} \mathbf{x} \\ \tau \end{bmatrix}$. Its LS solution is

$$\hat{\boldsymbol{\xi}}_{LS} = \mathbf{N}_{\xi}^{-1}\mathbf{w}_{\xi} \tag{15}$$

where

$$\mathbf{N}_{\xi} = \mathbf{H}^T\mathbf{Q}_{IF}^{-1}\mathbf{H} = \mathbf{e}_3^T\left(\mathbf{T}\Lambda\mathbf{T}^T\right)^{-1}\mathbf{e}_3 \times \begin{bmatrix} \mathbf{A}^T\mathbf{Q}_{DD}^{-1}\mathbf{A} & \mathbf{A}^T\mathbf{Q}_{DD}^{-1}\mathbf{b} \\ \mathbf{b}^T\mathbf{Q}_{DD}^{-1}\mathbf{A} & \mathbf{b}^T\mathbf{Q}_{DD}^{-1}\mathbf{b} \end{bmatrix} \tag{16a}$$

$$\mathbf{w}_{\xi} = \mathbf{H}^T\mathbf{Q}_{IF}^{-1}\mathbf{y}_{IF} = \begin{bmatrix} \mathbf{e}_3^T\left(\mathbf{T}\Lambda\mathbf{T}^T\right)^{-1}\otimes\mathbf{A}^T\mathbf{Q}_{DD}^{-1} \\ \mathbf{e}_3^T\left(\mathbf{T}\Lambda\mathbf{T}^T\right)^{-1}\otimes\mathbf{b}^T\mathbf{Q}_{DD}^{-1} \end{bmatrix}\mathbf{y}_{IF} \tag{16b}$$

The subscript "LS" denotes the LS solution. The covariance matrix of LS estimates is

$$\boldsymbol{\Sigma}_{\hat{\xi}_{LS}} = \sigma_0^2\mathbf{N}_{\xi}^{-1} \tag{17}$$

Since equation (14) is seriously ill-conditioned, the LS solution (15) and its corresponding covariance matrix (17) are rather instable and usually not admissible. In most cases, the LS solution (15) is even worse than LS solution from model without RZTD which is given as

$$\hat{\mathbf{x}}_{LS} = \mathbf{N}_{\mathbf{x}}^{-1}\mathbf{w}_{\mathbf{x}} \tag{18}$$

where

$$\mathbf{N}_{\mathbf{x}} = \mathbf{e}_3^T\left(\mathbf{T}\Lambda\mathbf{T}^T\right)^{-1}\mathbf{e}_3 \times \mathbf{A}^T\mathbf{Q}_{DD}^{-1}\mathbf{A} \tag{19a}$$

$$\mathbf{w}_{\mathbf{x}} = [\mathbf{e}_3^T\left(\mathbf{T}\Lambda\mathbf{T}^T\right)^{-1}\otimes\mathbf{A}^T\mathbf{Q}_{DD}^{-1}]\mathbf{y}_{IF} \tag{19b}$$

The corresponding covariance matrix of estimates is

$$\boldsymbol{\Sigma}_{\hat{\mathbf{x}}_{LS}} = \sigma_0^2\mathbf{N}_{\mathbf{x}}^{-1} \tag{20}$$

In the LS solution without RZTD, the residual tropospheric delays are ignored and the positional estimates are biased although the biases are small. However, ignoring the tropospheric delays can slightly affect the covariance matrix (20) which is understood well in context of LS adjustment since the RZTD is very small. Moreover the benefit of this solution is that the normal matrix (19a) is rather well conditioned. Therefore, the covariance matrix (20) is still a reasonable measure for its LS estimates (18).

3. Regularization-Based Troposphere Decorrelation

[23] The issue is to solve the ill-posed problem (14) to obtain reliable RTK position estimation. We employ regularization method proposed by *Tikhonov* [1963], which has been frequently used for solving inverse ill-posed problems in different fields, referring to *Xu* [1992] and *Xu and Rummel* [1994] for gravitational field inverse and *Shen and Li* [2007], *Ou and Wang* [2004], and *Li and Shen* [2008] regarding fast GPS ambiguity resolution.

3.1. Regularized Solution

[24] In ill-posed model (14), a small error in the observation $\mathbf{y}_{IF}$ will cause large error in the LS solution $\hat{\boldsymbol{\xi}}_{LS}$, according to the spectrum expression of solution equation (15) [see e.g., *Xu*, 1992; *Shen and Li*, 2007] (also refer to the results in section 4). The regularization is to stabilize the solution of an ill-posed model based on the criterion

$$\left(\mathbf{H}\hat{\boldsymbol{\xi}}_R - \mathbf{y}_{IF}\right)^T\mathbf{Q}_{IF}^{-1}\left(\mathbf{H}\hat{\boldsymbol{\xi}}_R - \mathbf{y}_{IF}\right) + \alpha\hat{\boldsymbol{\xi}}_R^T\mathbf{S}\hat{\boldsymbol{\xi}}_R = \min \tag{21}$$

where the subscript "$_R$" denotes a regularized solution. The positive constant α and positive (semi)definite matrix **S** are regularization parameter and regularization matrix, respectively, and both are important in the regularization. The ill condition of equation (14) is attributed to a strong correlation between RZTD and height. Hence we choose regularization matrix

$$\mathbf{S} = \begin{bmatrix} \mathbf{E}_3 & 0 \\ 0 & 0 \end{bmatrix} \tag{22}$$

and the regularized solution under the cost function (21) are derived as

$$\hat{\boldsymbol{\xi}}_R = \mathbf{N}_R^{-1}\mathbf{w}_{\xi} \tag{23}$$

where $\mathbf{N}_R = \mathbf{N}_{\xi} + \alpha\mathbf{S}$. The covariance matrix is derived according to the law of error propagation as

$$\boldsymbol{\Sigma}_{\hat{\xi}_R} = \sigma_0^2\mathbf{N}_R^{-1}\mathbf{N}_{\xi}\mathbf{N}_R^{-1} \tag{24}$$

The regularized solution (23) is more stable than the LS solution (17). However, as a trade-off, a bias is introduced in the regularized solution which can be computed as

$$\nabla\hat{\boldsymbol{\xi}} = \mathrm{E}\left(\hat{\boldsymbol{\xi}}_R - \boldsymbol{\xi}\right) = -\alpha\mathbf{N}_R^{-1}\mathbf{S}\overline{\boldsymbol{\xi}} \tag{25}$$

where E ( ) is a expectation operation; $\overline{\boldsymbol{\xi}} = \begin{bmatrix} \overline{\mathbf{x}} \\ \overline{\tau} \end{bmatrix}$ is the "true" value of parameter vector but in fact impossibly known. The mean square error (MSE) is used to evaluate the regularized solution including its bias effect,

$$\begin{aligned}\mathbf{M}_R &= \mathrm{E}\left[\left(\hat{\boldsymbol{\xi}}_R - \boldsymbol{\xi}\right)\left(\hat{\boldsymbol{\xi}}_R - \boldsymbol{\xi}\right)^T\right] = \boldsymbol{\Sigma}_{\hat{\xi}_R} + \nabla\hat{\boldsymbol{\xi}}\nabla\hat{\boldsymbol{\xi}}^T \\ &= \sigma_0^2\mathbf{N}_R^{-1}\mathbf{N}_{\xi}\mathbf{N}_R^{-1} + \alpha^2\mathbf{N}_R^{-1}\mathbf{S}\overline{\xi}\overline{\xi}^T\mathbf{S}\mathbf{N}_R^{-1}\end{aligned} \tag{26}$$

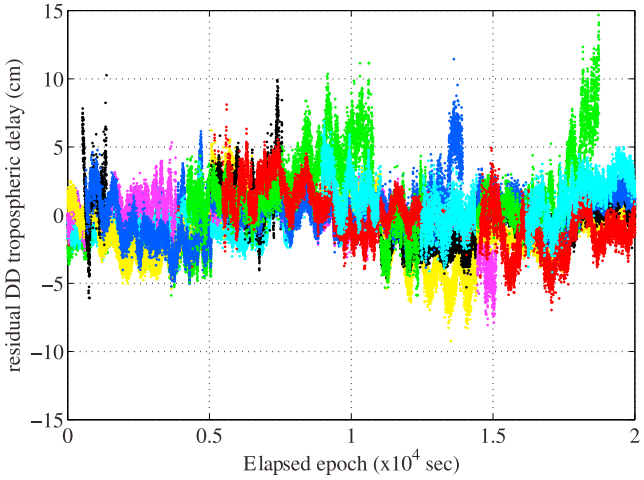

Figure 1. The residual DD tropospheric delays.

It is noticed that the regularization criterion (21) appears similar to or same as the Bayesian principle which was applied in the adaptive Kalman filter [*Yang et al.*, 2001] and the adaptive collocation [*Yang et al.*, 2009]. However, they are essentially different. In the Bayesian principle, **S** is the inverse of the prior covariance matrix of parameter and α is called adaptive factor used to balance the contributions of the observations and the prior information of parameter to the final estimate. More importantly the Bayesian estimate is unbiased because the adaptive factor is solved based on the variance component estimation theory. More information on the differences between regularization and Bayesian estimation is referred to *Xu et al.* [2007].

3.2. Geometry-Specified Regularization Parameter Determination

[25] It is observed from equation (23) that the regularization parameter is a prerequisite for computing the regularized solution. The optimal regularized solution can be obtained by finding the MSE minimum, which is equivalent to minimizing the trace of MSE matrix $\mathbf{M}_R$ [*Xu*, 1992; *Teunissen*, 2008; *Shen and Li*, 2007]. Therefore, the regularization parameter is computed based on the criterion that

$$\alpha = \arg\min_{\alpha>0} \operatorname{trace}(\mathbf{M}_R) \tag{27}$$

For more information on numerical computation of (27), one can refer to *Xu* [1992]. In fact, there are different criteria to compute the regularization parameter for the different purposes. The MSE minimization criterion is chosen because we concern the high-quality solution much more. From the frequentist point of view, the regularization parameter is employed to efficiently mitigate the effects of the high-frequency noises on the solution while almost not to decrease the contributions of the low-frequency signals to the solution [*Xu*, 1992; *Xu and Rummel*, 1994]. Once the regularization parameter α is determined, the more stable regularized solution with respect to LS solution is trivially computed by substituting it into equation (23). However, it is noticed from equation (26) that both variance component σ_0^2 and true values of unknowns $\overline{\xi}$ are involved in computing α. Thus, the reasonable variance component and true values of unknown should be first determined.

[26] The variance component σ_0^2 is crucial to determine α, because α is sensitive to the variation of σ_0^2. From theoretical point of view, α is used to essentially balance the contributions of observation and regularized bias in the regularized solution. If σ_0^2 is large, α will be generally larger as well, which will definitely lead to a larger bias. Conversely, if σ_0^2 is small, α will be also smaller, which means that ill condition cannot be efficiently controlled and the regularized solution remains unstable. Fortunately, in our technique, σ_0^2 is not involved to compute α; see the following for details. Hence, the most important factor is how to determine a reasonable substitute for the true values of unknowns.

[27] Normally, the true values $\overline{\boldsymbol{\xi}}$ of unknowns can be replaced by their LS estimates (15). The problem is that the LS solution (15) as well as its covariance matrix (17) are instable themselves in such ill-posed model, which is exactly why the regularization is used. Alternatively, one can conservatively initialize a small regularization parameter α to compute regularized solution. This solution is then used to replace $\overline{\boldsymbol{\xi}}$, from which a better α is computed. Using this computed α, a better regularized solution can be estimated to replace $\overline{\boldsymbol{\xi}}$. Continuing the iteration process would lead to the optimal regularized solution. However, in GPS real-world observation scenarios, the degree of the ill condition status of model (14) varies in the different observation periods and different observation geometry. Furthermore, iterative computation may increase the computation burden to an unbearable level for RTK applications.

[28] As mentioned in section 2.4, the LS solution without RZTD (18) is stable and generally better than that from (15) although it is slightly biased. Hence it is reasonable to replace the true value $\overline{\mathbf{x}}$ using $\hat{\mathbf{x}}_{LS}$. Analogously, we conclude from equation (26) that a larger $\overline{\mathbf{x}}$ deduces a smaller regularization parameter α and vice versa. This also applies to $\hat{\mathbf{x}}_{LS}$ as it is used to replace $\overline{\mathbf{x}}$. In this case, iterative approach

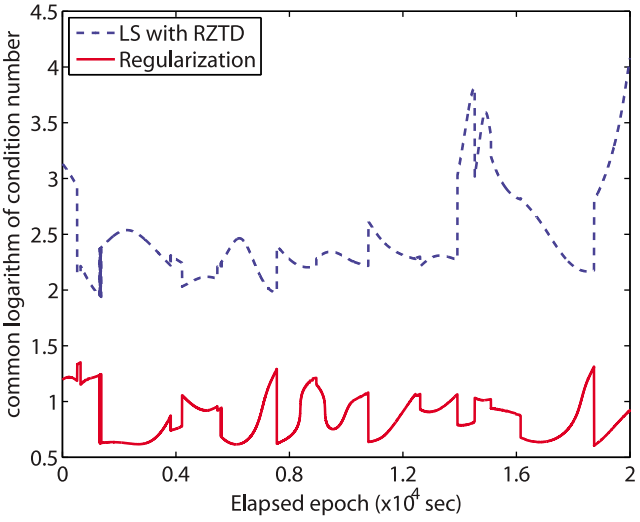

Figure 2. Condition numbers of normal matrices from regularization and LS with RZTD.

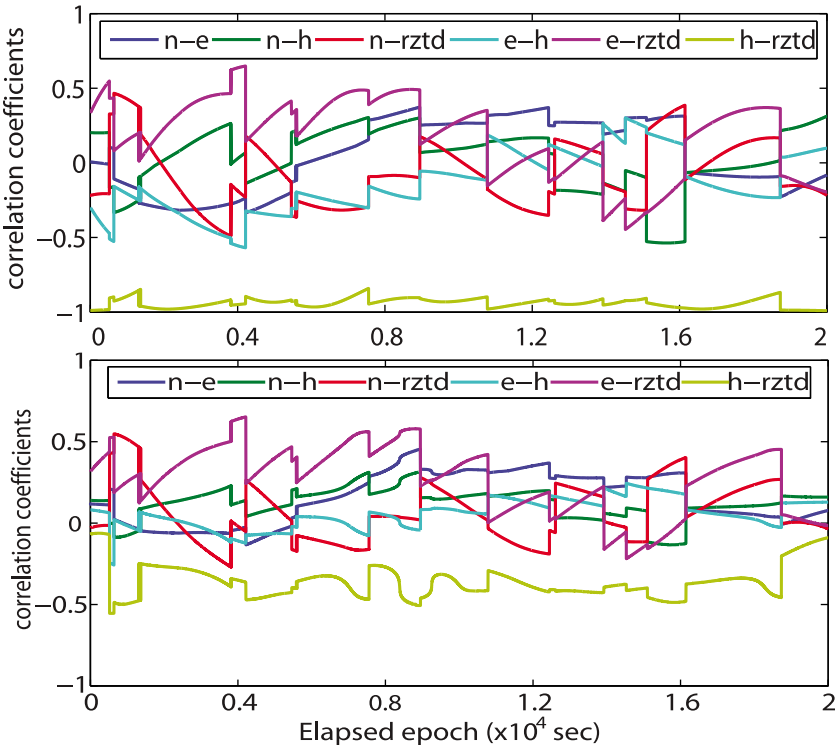

Figure 3. Correlation coefficients between all parameters of each other for (top) LS and (bottom) regularization.

is often used to compute $\hat{\mathbf{x}}_{LS}$ in order to reduce its value which results $\hat{\mathbf{x}}_{LS}$ being very close to zero. If we simply substitute it into equation (27) to compute α, a very large α will definitely be obtained. This significantly reduces the contribution of observations and the result is largely smoothed that it does not reflect the real-world situation properly. We notice that the covariance matrix (20) is a still reasonable measure for $\hat{\mathbf{x}}_{LS}$ as mentioned above. Hence, we propose to replace the quadratic matrix $\overline{\mathbf{x}\mathbf{x}}^T$ in equation (26) with the covariance matrix $\mathbf{\Sigma}_{\hat{\mathbf{x}}_{LS}}$ of LS solution $\hat{\mathbf{x}}_{LS}$, namely,

$$\mathbf{S}\overline{\xi\xi}^T\mathbf{S} = \begin{bmatrix} \mathbf{\Sigma}_{\hat{\mathbf{x}}_{LS}} & 0 \\ 0 & 0 \end{bmatrix} = \sigma_0^2 \begin{bmatrix} \mathbf{N}_{\mathbf{x}}^{-1} & 0 \\ 0 & 0 \end{bmatrix} = \sigma_0^2 \mathbf{Q}_{\mathbf{x}} \tag{28}$$

then

$$\mathbf{M}_R = \sigma_0^2\left(\mathbf{N}_R^{-1}\mathbf{N}_{\boldsymbol{\xi}}\mathbf{N}_R^{-1} + \alpha^2\mathbf{N}_R^{-1}\mathbf{Q}_{\mathbf{x}}\mathbf{N}_R^{-1}\right) = \sigma_0^2\mathbf{Q}_R \tag{29}$$

and the criterion (27) for α determination becomes

$$\alpha = \arg\min_{\alpha>0} \operatorname{trace}(\mathbf{Q}_R) \tag{30}$$

For this proposed technique, variance component is free of involvement in the α computation. It is emphasized that covariance matrix $\mathbf{\Sigma}_{\hat{\mathbf{x}}_{LS}}$ of position parameters from LS estimation without RZTD is essentially specified by the observation geometry. Therefore, the regularization parameter can be adaptively computed to specify the observation geometry variation. Once a reasonable α is achieved, the correlation between RZTD and height can be efficiently reduced.

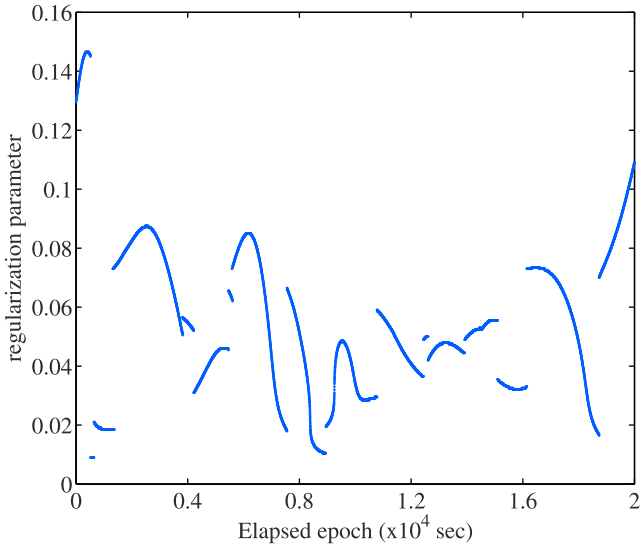

Figure 4. The computed regularization parameters.

Table 1. Mean Correlation Coefficients Between Any Two Parameters With Each Other for LS and Regularization (RG)

	n-e	*n-h*	*n-τ*	*e-h*	*e-τ*	*h-τ*
LS	0.046	0.030	−0.066	−0.134	0.183	−0.940
RG	0.036	0.005	−0.049	−0.057	0.152	−0.474

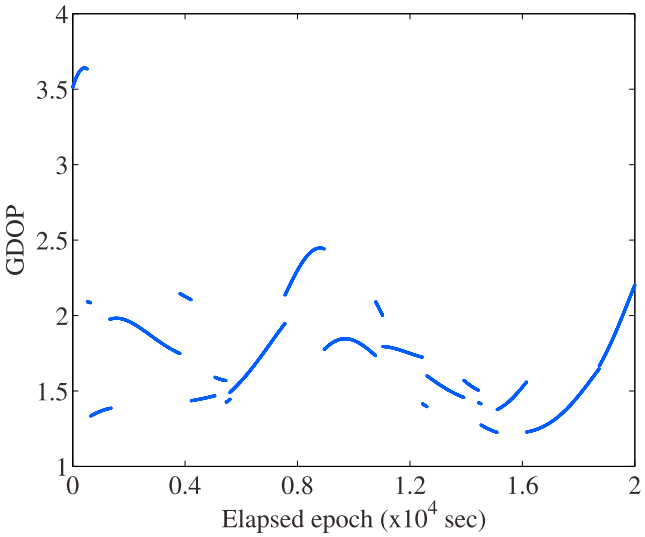

Figure 5. GDOP series in observation period.

3.3. Analysis of Regularization Bias

[29] In practice, it is desirable that the regularized bias as small as possible besides the stable regularized solution. In order to numerically compute the regularized bias, we use the regularized solution $\hat{\boldsymbol{\xi}}_R$ instead of the true values $\overline{\boldsymbol{\xi}}$ in equation (25),

$$\nabla\hat{\boldsymbol{\xi}}_R = -\alpha\mathbf{N}_R^{-1}\mathbf{S}\hat{\boldsymbol{\xi}}_R \tag{31}$$

Here the subscript "R" denotes the computed regularized bias using the regularized solution. The bias of the computed bias based on the regularized solution is derived as

$$\Delta\hat{\boldsymbol{\xi}}_R = \mathrm{E}\left(\nabla\hat{\boldsymbol{\xi}}_R - \nabla\boldsymbol{\xi}\right) = \alpha^2\mathbf{N}_R^{-1}\mathbf{S}\mathbf{N}_R^{-1}\mathbf{S}\overline{\boldsymbol{\xi}} \tag{32}$$

Obviously, it is a small value of second-order relative to the bias (25) itself. Thus, it is reasonable to evaluate the regularized bias using equation (31) based on the regularized solution.

4. Experiments and Analysis

[30] The dual-frequency GPS data were collected with sampling interval of 1 s in two CORS stations spacing 93.6 km in Guangzhou of China. There are a total of 20000 epochs collected with elevation mask set to 10°. The coordinates of two CORS stations are precisely known as the reference values for experiment comparison.

[31] First, we use our own research type Network RTK software to fix L1 and L2 DD ambiguities where the UNB3 standard tropospheric model is applied. The residual DD tropospheric delays are estimated using ambiguity-fixed ionosphere-free combinations with known coordinates, as illustrated in Figure 1. Each color denotes one pair of DD satellites. The residual tropospheric delays are significant, in particular for lower elevation observations. Thus, they must be carefully mitigated to obtain precise positioning.

[32] Condition number is a good measure for ill condition of a matrix. As Figure 2 shows, the mean magnitude of condition numbers of normal matrices (16a) is $10^{2.8}$, which proves the ill condition of model (14). Figure 3 presents the correlation coefficients between all parameters of each other. The strong correlation between height and RZTD is indeed existent with mean coefficient up to −0.94.

[33] In order to obtain a stable solution in such an ill-posed model, we use regularization method and compute regularization parameters according to equation (30). The results are shown in Figure 4. They show significant variations, indicating that if iterative regularization computation is used as described in section 3.2, the initial regularization parameter is difficult to choose. Referring to Figures 2 and 3, the condition number and correlation coefficients are efficiently reduced after regularization (also see Table 1). The means of condition numbers and correlation coefficients between height and RZTD are reduced from $10^{2.8}$ to $10^{0.9}$, and from −0.94 to −0.474, respectively. Thus it demonstrates that the regularization can efficiently mitigate the ill condition of model (14).

[34] Despite the large variation of regularization parameters over the whole observation period, the variations over short periods are very smooth. This is mainly due to the smooth variation of observed geometry over these short periods (see, e.g., Figure 5 of GDOP series). In general, a jump of regularization parameters is corresponding to the sudden change of GDOP values, and regularization parameter becomes larger with the increasing GDOP values, although at different rates. It means that a large regularization parameter is computed to efficiently mitigate the serious ill condition of model (14) which corresponds to large GDOP. Thus, the proposed method for regularization parameter determination

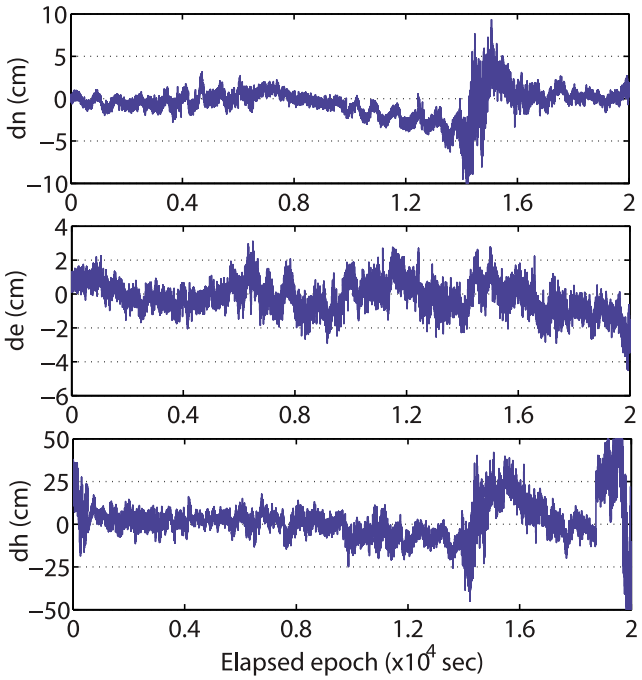

Figure 6. Differences between LS estimates with RZTD and their reference coordinates.

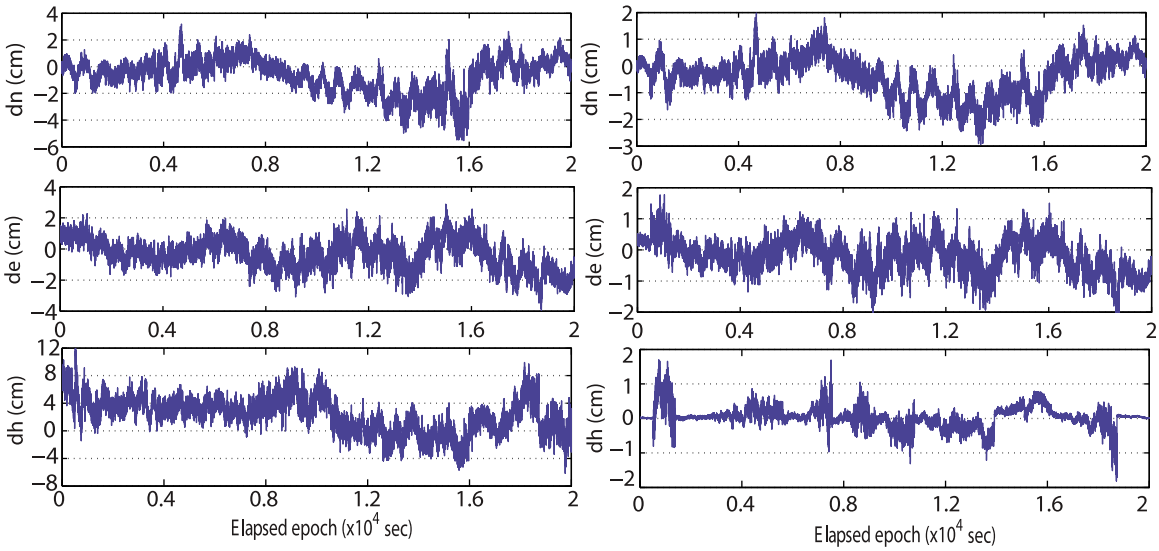

Figure 7. Coordinate differences relative to the reference for (left) the LS without RZTD and (right) the regularization technique.

can adaptively specify the observation geometry and then efficiently improve the characteristics of model (14).

[35] Now, we evaluate the regularized solution. First, the LS estimates are solved by equation (15), and their differences relative to the reference coordinates are shown in Figure 6. The magnitudes of difference series for *n*, *e*, and *h* components are 10 cm, 6 cm, and 50 cm, respectively. As stated above, they are generally worse than those from equation (18) without RZTD due to the ill-posed normal matrix (16a) (see, e.g., Figure 7). Thus in the following, we only compare our regularized solution with LS without RZTD from equation (18). The coordinate differences with respective to the reference are illustrated in Figure 7 for the LS and the regularization methods. It is apparent that the coordinate differences of the regularization method are significantly smaller than those of the LS. For horizontal components, the magnitudes of differences are roughly half of those in the LS. More promisingly, the regularization method can reduce the height differences from 12 cm to smaller than 2 cm, and for most cases smaller than 1 cm.

[36] We compute the statistical results for assessing the regularized solution. The means and root mean squared errors (RMS) precision of coordinate differences are presented in Table 2. Both means and RMSs for three components are significantly improved, and subcentimeter precisions are obtained. In particular, the mean of height component is almost equal to zero and the RMS is reduced from 3.48 cm to 0.31 cm. Such small mean and highly precise results are achieved due to the efficient separation of residual tropospheric delays from the coordinates, essentially attributing to epoch-by-epoch estimation of RZTDs which is shown in Figure 8. The actual RZTDs are previously estimated in Network RTK program along with ambiguity resolution based on a Kalman filtering procedure. Observing Figure 8, the regularized RZTDs are rather consistent with the actual ones. Importantly, it is well-known that RZTD from a filtering procedure is a smoothed (roughly averaged) RZTD of multiple epochs and thus cannot fully describe the instantaneous variation of the real RZTD. On the other hand, in our regularization approach, RZTD is estimated independently without filtering over epochs. Therefore it is capable of achieving the more accurate and highly dynamic RZTD estimates which provide the high precise height solution.

[37] We further analyze the improvement efficiency of our regularization for the height component over the different error intervals of LS solutions. Giving an error interval, we compute RMSs using all LS height estimates with errors in this error interval and their corresponding regularized estimates, respectively. Four error intervals of LS height estimates, smaller than 2 cm, from 2 cm to 5 cm, from 5 cm to 8 cm and larger than 8 cm, are used for statistical comparison. The results are shown in Table 3. With the value of error interval increasing, the LS RMS is increased significantly, but the regularization RMS is almost invariant. This implies that the regularization method can substantially improve the height solution almost independent of observation scenario.

[38] As mentioned in section 3.3, a good regularized solution should also possess a small bias besides a stable solution. The approximate biases of our regularized estimates are computed by using equation (31) and shown in Figure 9. In general, biases of the four parameters are in millimeter level, except for some epochs. Particularly, biases of the RZTD estimates are always smaller than 4 mm. The means of all biases are 1.5 mm, 0.4 mm, −0.2 mm and −0.1 mm for *n*, *e*, *h* coordinates and RZTD, respectively. These small biases are considered to be too small to have any influence on the regularized solution and thus ignored. Therefore, our

Table 2. Mean and RMS of Coordinate Differences for LS and RG

	Mean (cm)		RMS (cm)	
	LS	RG	LS	RG
n	−0.69	−0.41	1.47	0.85
e	−0.35	−0.20	1.03	0.58
h	2.34	0.04	3.48	0.31

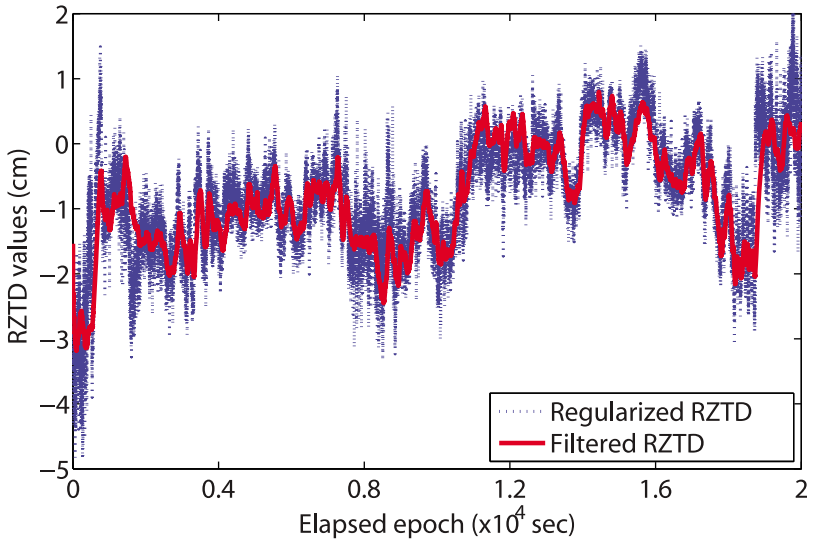

Figure 8. Comparison of regularized RZTDs and actual ones.

regularization method is efficient and can indeed improve the long-range RTK precision.

5. Conclusion and Remarks

[39] To address the applications of high-rate kinematic GPS solutions in geosciences, the issues for subcentimeter long-range RTK positioning has been intensively studied in this paper. A relative ZTD parameter is introduced along with the coordinate parameters to compensate the residual tropospheric delays. Importantly these parameters are solved using the regularization method as an ill-posed inverse problem independently from epoch to epoch. The key has been to compute the regularization parameter, then derive an optimal regularized solution using the "true" values of unknown parameters which however are unknown. The paper uses the covariance matrix of coordinates from LS without RZTD to replace the quadratic form of "true" values since it is stable and almost admissible with its LS solution. As a result, the regularization parameter is adaptively computed specifying the variation of observation geometry, and the correlation between RZTD and height is effectively reduced. It results in the subcentimeter positional precision. Moreover, millimeter level precision in height has been obtained.

[40] The experiment results from a 93.6 km baseline have shown that geometry-based positioning model with RZTD is seriously ill-conditioned mainly due to the strong correlation between height and RZTD with a mean correlation coefficient of −0.94. Thus the LS estimates are instable and always worse than those from the model without RZTD. It has shown that the adaptively computed regularization parameters based on our geometry-specified regularization method can indeed characterize the variation of observation geometry. Hence the model's ill condition can be efficiently and adaptively alleviated, showing that the means of condition numbers of normal equations and correlation coeffi-

Table 3. RMSs of LS and RG Height Estimates in Different Error Intervals

	LS Error Intervals (cm)			
Methods	<2	2–5	5–8	>8
LS	1.14	3.68	4.66	8.96
RG	0.29	0.29	0.41	0.29

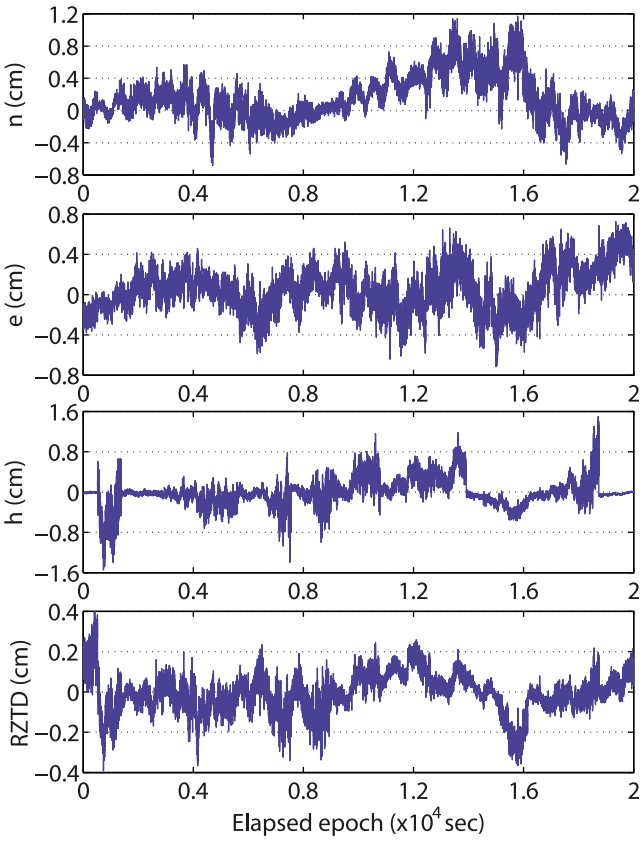

Figure 9. Computed biases of all parameters for all epochs based on the regularized solution.

cients between the height and the RZTD are reduced from $10^{2.8}$ to $10^{0.9}$ and from −0.94 to −0.474, respectively. Comparing with the LS solution, the proposed regularization method can improve the positioning precision to subcentimeter. Particularly, for the height component, the RMS precision is improved from 3.48 cm to 3.1 mm due to the real-time precise estimation of RZTD without the use of any filtering or smoothing strategies.

[41] Referring to the applications of high-rate GPS observations cited in section 1, the subcentimeter long-range RTK capability may have certain impact in geodesy and geophysics. Because the precision of the geoid determination has been improved to the millimeter level with the development of gravity satellite missions, such as CHAMP, GRACE as well as the latest GOCE [*Hofmann-Wellenhof and Moritz*, 2006, p.171], the bottleneck of GPS leveling is the precision of RTK height solution. With the proposed method, it is possible to obtain the millimeter-level RTK height solution in GPS leveling, which is in consistent with the most advanced geoid precision. In addition, the high-resolution precise RZTD estimations from epoch to epoch may have combined the effects of residual troposphere and multipath errors. It is therefore possible to understand the multipath behavior through analysis the high-resolution RZTDs against the low-resolution RZTD time series routinely obtainable from the International GNSS Services data analysis centers. Finally, the regularization method can be trivially applied to the other related GNSS positioning techniques, such as precise point positioning, multiple frequency GNSS positioning as well as network RTK positioning.

[42] **Acknowledgments.** This work is supported by Cooperative Research Centre for Spatial Information (CRC-SI) project 1.04 for regional GNSS positioning, the National Natural Science Funds of China (grant 40874016) as well as the Key Laboratory of Advanced Engineering Surveying of SBSM (grant TJES0809).

References

Ahn, Y., D. Kim, P. Dare, and J. Park (2008), Estimation of troposphere decorrelation using the combing zenith-dependent parameter, paper presented at ION GNSS 2008, Inst. of Navig., Savannah, Ga.

Bock, Y., L. Prawirodirdjo, and T. Melbourne (2004), Detection of arbitrarily large dynamic ground motions with a dense high-rate GPS networks, *Geophys. Res. Lett.*, *31*, L06604, doi:10.1029/2003GL019150.

Chen, W., C. Hu, Y. Chen, and X. Ding (2001), Rapid static and kinematic positioning with Hong Kong GPS active network, paper presented at ION GPS 2001, Inst. of Navig., Salt Lake City, Utah, 11–14 Sept.

Chen, X., S. Han, C. Rizos, and P. Goh (2000), improving real time positioning efficiency using the Singapore Integrated Multiple Reference Station Network (SIMRSN), paper presented at 13th International Technical Meeting, Satell. Div., Inst. of Navig., Salt Lake City, Utah, 19–22 Sept.

Collins, J., and B. Langley (1997), A tropospheric delay model for the user of the wide area augmentation system, *Tech. Rep.*, *187*, Dep. of Geod. and Geomat. Eng., Univ. of New Brunswick, Fredericton, Canada.

Dai, L., J. Wang, C. Rizos, and S. Han (2003), Predicting atmospheric biases for real-time ambiguity resolution in GPS/GLONASS reference station networks, *J. Geod.*, *76*, 617–628, doi:10.1007/s00190-002-0286-1.

Dodson, A., P. Shardlow, L. Hubbard, G. Elgered, and P. Jarlemark (1996), Wet tropospheric effects on precise relative GPS height determination, *J. Geod.*, *70*, 188–202, doi:10.1007/BF00873700.

Feng, Y., and B. Li (2008), A benefit of multiple carrier GNSS signals: Regional scale network-based RTK with doubled inter-station distances, *J. Spatial Sci.*, *53*(1), 135–147.

Feng, Y., and B. Li (2010), Wide area real time decimetre positioning services using triple frequency GNSS signals, *Sci. China D Earth Sci.*, *53*(5), 731–740, doi:10.1007/s11430-010-0032-0.

Frei, E., and G. Beutler (1990), Rapid static positioning based on the fast ambiguity resolution approach 'FARA': Theory and first results, *Manuscr. Geod.*, *15*, 326–356.

Gendt, G., G. Dick, C. H. Reigber, M. Tomassini, Y. Liu, and M. Ramatschi (2003), Demonstration of NRT GPS water vapor monitoring for numerical weather prediction in Germany, *J. Meteorol. Soc. Jpn.*, *82*(1B), 360–370.

Genrich, J., and Y. Bock (1992), Rapid resolution of crustal motion at short ranges with the global positioning system, *J. Geophys. Res.*, *97*(B3), 3261–3269, doi:10.1029/91JB02997.

Grejner-Brzezinska, D., I. Kashani, and P. Wielgosz (2005), On accuracy and reliability of instantaneous network RTK as a function of network geometry, station separation, and data processing strategy, *GPS Solut.*, *9*, 212–225, doi:10.1007/s10291-005-0130-1.

Hatch, R. (1990), Instantaneous ambiguity resolution, in *Kinematic Systems in Geodesy, Surveying, and Remote Sensing*, edited by K.-P. Schwarz and G. Lachapelle, *Int. Assoc. Geod. Symp.*, *107*, 299–308.

Hofmann-Wellenhof, B., and H. Moritz (2006), *Physical Geodesy*, 2nd ed., Springer, New York.

Hu, G., H. Khoo, P. Goh, and C. Law (2003), Development and assessment of GPS virtual reference stations for RTK positioning, *J. Geod.*, *77*, 292–302, doi:10.1007/s00190-003-0327-4.

Kim, D., and R. Langley (2008), Innovation: Improving long-range RTK, *GPS World*, 1 March. (Available at http://www.gpsworld.com/gnss-system/signal-processing/innovation-improving-long-range-rtk-4219)

Kim, D., S. Bisnath, R. Langley, and P. Dare (2004), Performance of long-baseline real-time kinematic applications by improving tropospheric delay modeling, paper presented at ION GNSS 17th International Technical Meeting of the Satellite Division, Inst. of Navig., Long Beach, Calif., 21–24 Sept.

Leick, A. (2004), *GPS Satellite Surveying*, 3rd ed., John Wiley, New York.

Li, B., and Y. Shen (2008), Prior baseline information based fast GPS ambiguity resolution, *Acta Geod. Cartogr. Sin.*, *37*(4), 423–427.

Li, B., and Y. Shen (2010), Global navigation satellite system ambiguity resolution with constraints from normal equations, *J. Surv. Eng.*, *136*(2), 63–71, doi:10.1061/(ASCE)SU.1943-5428.0000017.

Li, B., Y. Shen, and P. Xu (2008), Assessment of stochastic models for GPS measurements with different types of receivers, *Chin. Sci. Bull.*, *53*(20), 3219–3225, doi:10.1007/s11434-008-0293-6.

Li, B., Y. Feng, and Y. Shen (2010), Three carrier ambiguity resolution: Distance-independent performance demonstrated using semi-generated triple frequency GPS signals, *GPS Solut.*, *14*(2), 177–184, doi:10.1007/s10291-009-0131-6.

Niell, A. (1996), Global mapping functions for the atmosphere delay at radio wavelengths, *J. Geophys. Res.*, *101*(B2), 3227–3246, doi:10.1029/95JB03048.

Ou, J., and Z. Wang (2004), An improved regularization method to resolve integer ambiguity in rapid positioning using single frequency GPS receivers, *Chin. Sci. Bull.*, *49*(2), 196–200, doi:10.1360/03WD0210.

Schaffrin, B., and E. Grafarend (1986), Generating classes of equivalent linear models by nuisance parameter elimination, applications to GPS observations, *Manuscr. Geod.*, *11*, 262–271.

Schüler, T. (2006), Impact of systematic errors on precise long baseline kinematic GPS positioning, *GPS Solut.*, *10*, 108–125, doi:10.1007/s10291-005-0012-6.

Shen, Y., and B. Li (2007), Regularized solution to fast GPS ambiguity resolution, *J. Surv. Eng. 133*(4), 168–172, doi:10.1061/(ASCE)0733-9453(2007)133:4(168).

Shen, Y., and G. Xu (2008), Simplified equivalent representation of GPS observation equations, *GPS Solut.*, *12*, 99–108, doi:10.1007/s10291-007-0070-z.

Shen, Y., B. Li, and G. Xu (2009), Simplified equivalent multiple baseline solutions with elevation dependent weights, *GPS Solut.*, *13*(3), 165–171, doi:10.1007/s10291-008-0109-9.

Shi, C., Y. Lou, H. Zhang, Q. Zhao, J. Geng, R. Wang, R. Fang, and J. Liu (2010), Estimating seismic displacement of the M_w8.0 Wenchuan earthquake from high-rate GPS observations, *Adv. Space Res.*, *46*(2), 228–235, doi:10.1016/j.asr.2010.03.006.

Teunissen, P. (1995), The least-squares ambiguity decorrelation adjustment: A method for fast GPS integer ambiguity estimation, *J. Geod.*, *70*, 65–82, doi:10.1007/BF00863419.

Teunissen, P. (2008), On a stronger-than-best property for best prediction, *J. Geod.*, *82*, 167–175, doi:10.1007/s00190-007-0169-6.

Tikhonov, A. (1963), Regularization of ill-posed problems, *Dolk. Akad. Nauk. SSSR, Engl. Transl.*, *151*(1), 49–52.

Tralli, D., and S. Lichten (1990), Stochastic estimation of tropospheric path delays in Global Positioning System geodetic measurements, *Bull. Geod.*, *64*, 127–159, doi:10.1007/BF02520642.

Wielgosz, P., I. Kashani, and D. Grejner-Brzezinska (2005), Analysis of long-range network RTK during a severe ionospheric storm, *J. Geod.*, *79*, 524–531, doi:10.1007/s00190-005-0003-y.

Xu, G. (2002), GPS data processing with equivalent observation equations, *GPS Solut.*, *6*(1–2), 28–33, doi:10.1007/s10291-002-0009-3.

Xu, P. (1992), Determination of surface gravity anomalies using gradiometric observables, *Geophys. J. Int.*, *110*, 321–332, doi:10.1111/j.1365-246X.1992.tb00877.x.

Xu, P., and R. Rummel (1994), A simulation study of smoothness methods in recovery of regional gravity fields, *Geophys. J. Int.*, *117*, 472–486, doi:10.1111/j.1365-246X.1994.tb03945.x.

Xu, P., Y. Shen, Y. Fukuda, and Y. Liu (2007), Reply to the comments by K. R. Koch and J. Kusche on Xu et al. (2006) Variance component estimation in linear inverse ill-posed models, J Geod 80:69–81, *J. Geod.*, *81*, 633–635, doi:10.1007/s00190-007-0164-y.

Yang, Y., H. He, and G. Xu (2001), Adaptively robust filtering for kinematic geodetic positioning, *J. Geod.*, *75*, 109–116, doi:10.1007/s001900000157.

Yang, Y., A. Zeng, and J. Zhang (2009), Adaptive collocation with application in height system transformation, *J. Geod.*, *83*, 403–410, doi:10.1007/s00190-008-0226-9.

Zhang, J., and G. Lachapelle (2001), Precise estimation of residual tropospheric delays using a regional GPS network for real-time kinematic applications, *J. Geod.*, *75*, 255–266, doi:10.1007/s001900100171.

Y. Feng and C. Wang, Faculty of Science and Technology, Queensland University of Technology, Brisbane, Qld 4001, Australia.

B. Li, Department of Surveying and Geo-informatics Engineering, Tongji University, 1239 Siping Rd., Shanghai 200092, China. (bofeng_li@163.com)

Y. Shen, Key Laboratory of Advanced Surveying Engineering of State Bureau of Surveying and Mapping, 1239 Siping Rd., Shanghai 200092, China.